Volume 8
Number 1
January 2020
Pages 1-520

# Biomaterials Science

rsc.li/biomaterials-science

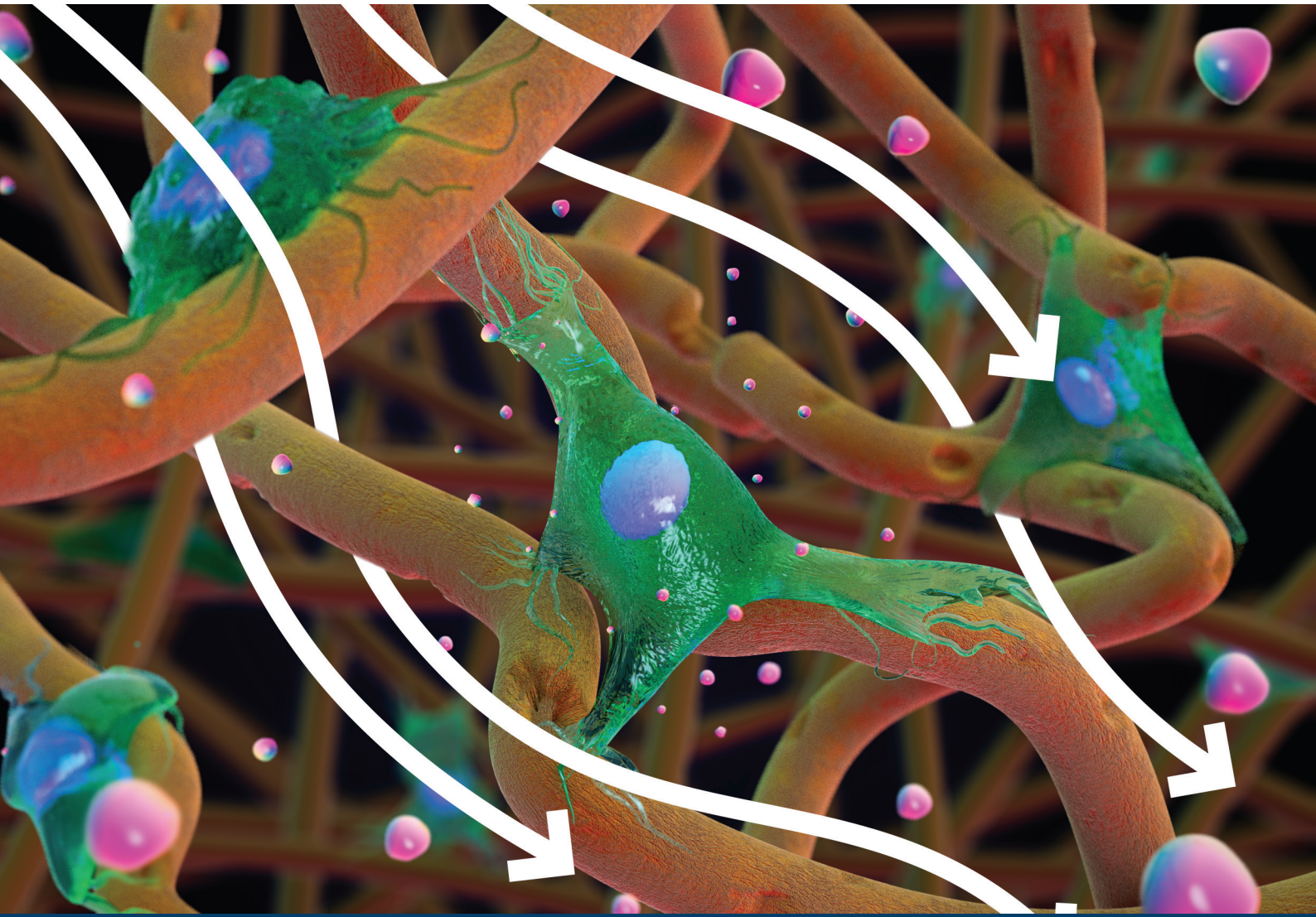

Themed issue: 29th Annual Conference of the European Society for Biomaterials

ISSN 2047-4849

ROYAL SOCIETY OF CHEMISTRY

**PAPER**
Carlijn V. C. Bouten, Anthal I. P. M. Smits *et al.*
Hemodynamic loads distinctively impact the secretory profile of biomaterial-activated macrophages – implications for *in situ* vascular tissue engineering

European Society for Biomaterials

Biomaterials Science

PAPER

View Article Online
View Journal | View Issue



Cite this: *Biomater. Sci.*, 2020, **8**, 132

# Hemodynamic loads distinctively impact the secretory profile of biomaterial-activated macrophages – implications for *in situ* vascular tissue engineering†

Tamar B. Wissing, [a,b] Eline E. van Haaften, [a,b] Suzanne E. Koch, [a,b] Bastiaan D. Ippel, [a,b] Nicholas A. Kurniawan, [a,b] Carlijn V. C. Bouten *[a,b] and Anthal I. P. M. Smits *[a,b]

Biomaterials are increasingly used for *in situ* vascular tissue engineering, wherein resorbable fibrous scaffolds are implanted as temporary carriers to locally initiate vascular regeneration. Upon implantation, macrophages infiltrate and start degrading the scaffold, while simultaneously driving a healing cascade *via* the secretion of paracrine factors that direct the behavior of tissue-producing cells. This balance between neotissue formation and scaffold degradation must be maintained at all times to ensure graft functionality. However, the grafts are continuously exposed to hemodynamic loads, which can influence macrophage response in a hitherto unknown manner and thereby tilt this delicate balance. Here we aimed to unravel the effects of physiological levels of shear stress and cyclic stretch on biomaterial-activated macrophages, in terms of polarization, scaffold degradation and paracrine signaling to tissue-producing cells (*i.e.* (myo) fibroblasts). Human THP-1-derived macrophages were seeded in electrospun polycaprolactone bis-urea scaffolds and exposed to shear stress (~1 Pa), cyclic stretch (~1.04), or a combination thereof for 8 days. The results showed that macrophage polarization distinctly depended on the specific loading regime applied. In particular, hemodynamic loading decreased macrophage degradative activity, especially in conditions of cyclic stretch. Macrophage activation was enhanced upon exposure to shear stress, as evidenced from the upregulation of both pro- and anti-inflammatory cytokines. Exposure to the supernatant of these dynamically cultured macrophages was found to amplify the expression of tissue formation- and remodeling-related genes in (myo)fibroblasts statically cultured in comparable electrospun scaffolds. These results emphasize the importance of macrophage mechano-responsiveness in biomaterial-driven vascular regeneration.

Received 28th June 2019,
Accepted 25th October 2019

DOI: 10.1039/c9bm01005j

rsc.li/biomaterials-science



## 1. Introduction

Replacing damaged small-diameter arteries (*e.g.* peripheral arteries and arteriovenous shunts) using biomaterial-based grafts remains notoriously challenging as they often lack the required structure–function properties to guarantee long-term patency. To better emulate the performance of autologous conduits, synthetic vascular implants (*e.g.* scaffolds) are developed that exploit the regenerative potential of the host.[1,2] This approach, also known as *in situ* tissue engineering, hinges on the use of acellular, often synthetic, biodegradable scaffolds that provide a temporary instructive environment to support the formation of a living and functional neotissue at the locus of implantation. When implanted, the scaffold directly takes over tissue functionality, while simultaneously directing cellular infiltration, extracellular matrix (ECM) deposition and subsequent remodeling of the deposited ECM components to develop native structure–function properties.[1,2] Importantly, as the tissue regenerates, the scaffold should resorb in a controlled fashion in order to ensure sustained graft functionality, adequate mechanical stimulation of the scaffold-residing cells and concomitant maturation of the newly deposited tissue. Too quick degradation may result in impaired healing and loss of structural integrity, while prolonged scaffold presence might contribute to chronic inflammation and pathological tissue formation (*e.g.* scarring); all ultimately resulting in graft

[a]*Department of Biomedical Engineering, Eindhoven University of Technology, Eindhoven, The Netherlands. E-mail: c.v.c.bouten@tue.nl, a.i.p.m.smits@tue.nl; Tel: +31 40 247 3006, +31 40 247 4735*
[b]*Institute for Complex Molecular Systems (ICMS), Eindhoven University of Technology, Eindhoven, The Netherlands*

†Electronic supplementary information (ESI) available. See DOI: 10.1039/c9bm01005j

failure. As such, *in situ* tissue engineering places high demands on scaffold design and the biomaterials used.

Macrophages are the crucial conciliators in wound healing as well as the foreign body response to implanted biomaterials.[3–7] Consequently, macrophages are considered to be one of the directing cells in *in situ* vascular tissue engineering wherein they control both biomaterial degradation as well as tissue repair and regeneration, especially during the initial stages of regeneration.[1] By synthesizing large amounts of degrading hydrolytic enzymes and/or reactive oxygen species (ROS), macrophages actively contribute to enzyme-catalyzed hydrolytic as well as oxidative scaffold degradation.[8–11] In parallel, they secrete various bioactive paracrine factors (*e.g.* cytokines and growth factors) that control the behavior of tissue-producing cells (*e.g.* cellular attraction, migration, proliferation, and differentiation) and eventual ECM deposition and remodeling.[5,12–14] Which factors are secreted is determined by the macrophage phenotypical state, which in turn depends on the phase of tissue repair and the cellular microenvironment.[6,7] Herein, a rough division can be made between the pro-inflammatory M1 phenotype, important for host-defense, and the anti-inflammatory M2 phenotypes (*e.g.* M2a, M2b and M2c), that are involved in wound healing and immune regulation.[6,7] The M1/M2 ratio is widely accepted as a predictive measure for the long-term tissue outcome.[5,15] Yet, macrophages are plastic and may reverse their behavior as environmental circumstances change (*e.g.* due to biochemical, topographical, mechanical cues).[5] Moreover, macrophage-biomaterial interactions typically result in mixed macrophage phenotypes, expressing both pro- and anti-inflammatory markers simultaneously,[16,17] underlining the importance of including functional read-outs to better predict graft performance.

Another critical parameter in macrophage-directed tissue regeneration is the dynamic biomechanical environment (*i.e.* blood-flow-induced shear stress and blood-pressure-driven cyclic stretch). As the scaffold degrades and neo-tissue develops, hemodynamic loading on the scaffold-populating cells will change in a time-dependent fashion.[1,18] This mechanical loading has been shown to directly affect biomaterial degradation kinetics.[19] In addition, hemodynamic loads have been identified as important determinants of tissue regeneration and are known to dictate the structure–function properties of the newly formed tissue.[1,12,20–22] From an immunological perspective, increasing wall shear stresses can also influence cell adhesion as well as cell apoptosis.[23–25] Moreover, cyclic stretch is identified as an important mediator of monocyte-to-macrophage differentiation and results in differential expression of multiple degradative and bioactive compounds.[26–28]

Whereas the mechano-responsiveness of the macrophage is increasingly recognized,[29] little is known on the individual and combined effects of shear stress and cyclic stretch on macrophage phenotype and its consequent tissue stimulatory and degradative potential in scaffolds. Therefore, we aimed to systematically delineate the effects of physiological shear stress and cyclic stretch on early macrophage polarization, macrophage-driven biomaterial degradation and its related paracrine signaling to (myo)fibroblasts. To this end, THP-1-derived human macrophages were seeded into 3D electrospun biodegradable poly-caprolactone-bis-urea (PCL-BU) tubular scaffolds and exposed to either shear stress (~1 Pa), cyclic stretch (~1.04) or a combination of both (~1 Pa shear stress +~1.04 cyclic stretch) for 8 days. In parallel, human (myo)fibroblasts were seeded in similar scaffolds and exposed to the macrophage-conditioned media for 8 days to investigate the indirect effects of alterations in macrophage secretory profile on neotissue formation. Our results reveal distinct effects of shear stress, cyclic stretch and the combination thereof on both the macrophage phenotype and secretory profile and the downstream phenotype of (myo)fibroblasts.

## 2. Experimental section

### 2.1 Experimental outline

The study was divided into three parts. In the first part, cell-free experiments with solely fibrin-seeded tubular electrospun PCL-BU scaffolds were performed to assess the effect of physiological hemodynamic loading on the chemical and physical integrity of the scaffold using a custom-made bioreactor.[22] PCL-BU was chosen as the biomaterial of interest as it belongs to a class of elastomeric thermoplastic materials that is susceptible to enzymatic and oxidative degradation[11] and has demonstrated its potential for *in situ* cardiovascular tissue engineering applications.[30–34] Secondly, human THP-1 derived monocytes were seeded in comparable scaffolds (using fibrin as a cell carrier), stimulated to become macrophages and exposed to physiological loading conditions (shear stress, cyclic stretch or a combination thereof) for 8 days in the bioreactor. Statically cultured macrophage-seeded tubular scaffolds were included as experimental controls. Samples were evaluated with respect to macrophage phenotype (in terms of gene and protein expression) and macrophage degradative potential (quantified as oxidative stress and resorbed mass of the scaffolds). Simultaneously, macrophage-conditioned media were collected at day 4 and day 8 and used to determine protein content. The third part of the study was aimed at evaluating the paracrine tissue stimulatory and remodeling effects of the hemodynamically loaded macrophages on human (myo)-fibroblasts, in terms of cell proliferation, phenotype and ECM-related gene expression. To that end, human (myo)fibroblasts (human vena saphena cells, HVSCs) were seeded in PCL-BU scaffolds (using fibrin as a cell carrier), cultured and exposed to the conditioned media of the statically and dynamically cultured macrophages for 8 days. HVSCs-seeded scaffolds that were exposed to unconditioned medium were included as controls. Samples were processed for further analyses at day 4 (HVSCs samples) and/or day 8 (macrophage and HVSCs samples) to correlate hemodynamic load-directed macrophage behavior to biomaterial degradation and tissue regeneration. All experiments were performed at least twice to verify reproducibility.

### 2.2 Scaffold fabrication and characterization

Scaffold tubes (macrophage samples) or sheets (HVSCs samples) were electrospun from 15% (w/w) bis-urea-modified poly(ε-caprolactone) (PCL-BU, SyMO-Chem, Eindhoven, The Netherlands) and 85% (w/w) chloroform (Sigma; 372978) polymer solutions. The solutions were transferred (flow rate: 40 μL $min^{-1}$) through a charged needle (16 kV) towards a negatively charged, rotating 3 mm ∅ mandrel or 35 mm ∅ mandrel (−1 kV, 500 rpm or 100 rpm, needle-mandrel distance: 16 cm) in a climate-controlled cabinet (23 °C and 30% humidity, IME Technologies, Geldrop, The Netherlands). After spinning, scaffolds were dried under vacuum overnight to remove solvent remnants. Table 2 provides an overview of the chemical properties of the used PCL-BU electrospun material. Scaffolds were imaged with scanning electron microscopy (SEM) (low vacuum, 10 kV electron beam, Quanta 600F; FEI, Hillsboro, OR) to assess the microarchitecture (*i.e.*, fiber morphology, diameter, pore size, and distributions). The average fiber diameter and pore size were determined by 30 individual measurements of randomly chosen fibers/pores in two representative images of a scaffold tube or sheet using Image J software (U.S. National Institutes of Health, Bethesda, MD, USA). Before cell seeding, tubular scaffolds were mounted onto silicone tubing, sterilized by UV exposure (30 min per side), wetted in demineralized water, and incubated in THP-1 medium (Roswell Park Memorial Institute-1640 (RPMI-1640, Gibco, ref A10491) supplemented with 10% fetal bovine serum (FBS, Greiner, Alphen aan den Rijn, The Netherlands) and 1% penicillin/streptomycin (P/S, Lonza, Basel, Switzerland; DE17-602E)) overnight at 37 °C to allow for protein adsorption. Similarly, UV-sterilized electrospun sheets were cut in 10 × 10 mm scaffolds and incubated in HVSCs medium (advanced Dulbecco's modified Eagle's culture (a-DMEM; Gibco), enriched with 10% FBS, 1% GlutaMax (Gibco; ref 35050), and 1% P/S).

### 2.3 Cell culture

**2.3.1 THP-1 monocytes and HVSCs.** Human monocytes (THP-1) were cultured and expanded using a standard cell culture incubator (37 °C, 5% CO2) in THP-1 medium according to supplier's instructions. After initial expansion, cells were frozen in liquid nitrogen using DMSO-enriched freezing medium (10% DMSO). Prior to the experiments, cells were thawed and expanded to reach the required cell number. Medium was refreshed three times a week to keep cell densities consistent (0.5–1.5 × $10^6$ cells per mL of medium).

HVSCs from the saphenous vein were obtained from a human donor after coronary by-pass surgery in accordance to the "Code Proper Secondary Use of Human Tissue" developed by the Federation of Medical Societies (FMWV) in the Netherlands. Conform the Dutch medical scientific research with human subjects act (WMO), secondary usage of patient material does not require assessment by a Medical Ethics Examination Committee. Nevertheless, informed consent was obtained from patients, stored by the physician involved and the tissues were handed over anonymously, without any patient-specific information except for gender and age, to warrant patient privacy. The HVSCs were isolated conform standard protocols.[35] Cells were expanded in HVSCs medium in a standard cell culture incubator (37 °C, 5% CO2). Culture medium was renewed every 3–4 days and the cells were passaged at 80% confluency.

**2.3.2 Cell seeding.** Prior to cell seeding, culture medium was removed and either THP-1 monocytes (250 × $10^6$ cells per $cm^3$; passage 9–10 after thawing) or HVSCs (15 × $10^6$ cells per $cm^3$; passage 6) were carefully seeded on the tubular or rectangular PCL-BU scaffolds respectively using fibrin as a cell carrier.[36] In short, cells were suspended in a mixture of fibrinogen (bovine, 10 mg $mL^{-1}$, Sigma; F8630) and thrombin (bovine, 10 IU $mL^{-1}$, Sigma; T4648) and homogeneously dripped over the rectangular scaffold surface or over the full length of the tubular scaffold on both sides. The suspension was allowed to enter the scaffold and polymerize (30 min) in a general cell incubator (37 °C, 5% $CO_2$).

**2.3.3 Differentiation and dynamic culture of macrophages.** After fibrin polymerization, each monocyte-seeded scaffold was transferred to a 15 mL tube containing 10 mL of 50 ng $mL^{-1}$ phorbol 12-myristate 13-acetate (PMA, Sigma Aldrich, P8139)-enriched THP-1 medium to stimulate monocyte-to-macrophage differentiation for 2 days. Subsequently, PMA enriched medium was removed and replaced with THP-1 medium for 24 h. After the 24 h incubation period, the macrophage-seeded tubular scaffolds ($n \geq 6$ samples per group) were mechanically stimulated for 8 days. To this end, flow chambers were mounted and connected to pumps to generate cyclic stretch (~1.04 at 0.5 Hz) and shear stress (~1 Pa) as previously described.[22] These values were chosen as physiologically relevant levels of loading, which are to be expected when these scaffolds are exposed to the hemodynamic loading conditions when implanted as small-diameter peripheral arterial replacements in humans.

**2.3.4 Paracrine stimulation of HVSCs.** HVSCs-seeded scaffolds were placed in a 6-well plate and after fibrin polymerization the scaffolds were cultured for 2 days in 4 ml per scaffold HVSCs medium prior to paracrine stimulation. The media from the mechanically stimulated macrophages were collected at day 4 and 8 and centrifuged (150*g*, 5 min, 4 °C) to remove cellular remnants. The conditioned supernatants were pooled per experimental group, mixed in a 1 : 1 ratio with fresh HVSCs medium and added to the HVSCs seeded PCL-BU scaffolds (4 mL per sample, $n$ = 6 scaffolds per group per timepoint). Samples that received a mixture of fresh cell culture media (THP-1 medium : HVSCs medium (1 : 1)) were included as a control.

### 2.4 Analyses

At day 4 (HVSCs) and day 8 (macrophages, HVSCs and cell-free), the scaffolds were collected, washed in phosphate-buffered saline (PBS, 2 × 5 s) and divided according to the predefined cutting scheme (ESI Fig. S1†). The samples were either dried in vacuum overnight and stored at room temperature

 

(cell-free), fixed for 15 minutes in 3.7% formaldehyde, followed by a PBS washing step (3 × 5 min) and stored at 4 °C (macrophages and HVSCs), or snap-frozen in liquid nitrogen and stored at −30 °C (macrophages, HVSCs and cell-free) for further analysis. Macrophage number, morphology, phenotype, proliferation, and biomaterial degradation were assessed by DNA analysis, Ki67 staining, qPCR, malondialdehyde (MDA) quantification and scanning electron microscopy (SEM), respectively. Media from the macrophage cultures were collected, centrifuged (150*g*, 5 min, 4 °C) and supernatants were stored at −30 °C to quantify protein content (ELISA). The collected HVSCs samples were further processed to investigate the effects of the supernatants on HVSCs proliferation and phenotype (Ki67 staining, qPCR, DNA analysis). The dried cell-free samples were examined on mass loss, fiber morphology (SEM), and thermal behavior (differential scanning calorimetry (DSC)). The −30 °C samples were further processed to determine the molecular weights (gel permeation chromatography (GPC)).

**2.4.1 DNA quantification.** Macrophage and HVSCs samples were lyophilized, weighed and photographed to determine the surface area ($mm^2$, analyzed using ImageJ) and disrupted using a micro-dismembrator (Sartorius, Goettingen, Germany). In short, samples were transferred to Nalgene cryogenic vials (Thermo Scientific; 5000-0012) containing 3 mm ∅ beads (Sartorius, Goettingen, Germany), snap-frozen in liquid nitrogen and disrupted in the micro-dismembrator (2 × 30 s at 3000 rpm). After disruption, papain-enriched digestion buffer (100 mM phosphate buffer (pH = 6.5), 5 mM L-cysteine (C-1276), 5 mM ethylene-di-amine-tetra-acetic acid (EDTA, ED2SS), and 140 μg $mL^{-1}$ papain (P4762), all from Sigma-Aldrich) was added. Each sample powder was well-mixed in 500 μL of digestion buffer and transferred to a new Eppendorf tube for digestion at 60 °C (16 h, Thermomixer Compact F 1.6 A, VWR). After digestion, samples were stored at 4 °C until analysis. Prior to DNA quantification, samples were vortexed and centrifuged (12 000 rpm, 10 min) to mix and precipitate scaffold remnants respectively. DNA content was quantified using 10 μL (macrophages) or 20 μL (HVSCs) of the supernatant, the Qubit dsDNA broad range (macrophages) or high sensitivity (HVSCs) assay kit, and the Qubit fluorometer (Life Technologies) following manufacturer's instructions.

**2.4.2 Oxidative stress quantification: MDA assay.** Malondialdehyde (MDA) is a by-product of ROS-induced lipid peroxidation and was quantified (MDA assay kit, Sigma Aldrich, MAK085) in the macrophage samples as an indirect measure of ROS production, oxidative stress and potential oxidative biomaterial degradation. To correct for potential variations in the size of the analyzed sample, as cutting was performed manually, the scaffold area ($mm^2$) of each scaffold was determined prior to analysis (ImageJ). After sample disruption, as described in section 2.4.1, 300 μL of lysis buffer was added to each sample powder, mixed properly, and incubated for 5 minutes on ice. Subsequently, the lysis buffer was transferred to a new Eppendorf tube and centrifuged (10 min at 11 000 rpm) to precipitate insoluble particles. Of each sample, 200 μL of supernatant was mixed with 600 μL of thiobarbituric acid (TBA) to form a fluorometric product. These products were quantified in a microplate reader (Synergy HTX multimode-reader, Biotek) using an excitation/emission wavelength of 532/553 nm. Obtained values were corrected for the average DNA content per experimental group.

**2.4.3 Gene expression profiles: qPCR.** For RNA extraction, macrophage and HVSCs samples were disrupted (see section 2.4.1) and lysed on ice for 5 minutes using RLT lysis buffer containing β-mercaptoethanol (Sigma; M3148). RNA was isolated using the Qiagen RNeasy kit following supplier instructions including a 30 minutes DNAse incubation step (Qiagen; 74106) to remove genomic DNA contamination. After extraction, RNA quantity and purity were assessed with a spectrophotometer (NanoDrop, ND-1000, Isogen Life Science, The Netherlands). RNA integrity was checked with gel electrophoresis. cDNA was synthesized in a thermal cycler (protocol: 65 °C (5 min), on ice (2 min) while adding the enzyme mixture, 37 °C (2 min), 25 °C (1 min), 37 °C (50 min), and 70 °C (15 min)) starting from a 20 μL reaction solution containing 200 ng of RNA, 1 μL dNTPs (10 mM, Invitrogen), 1 μL random primers (50 ng $\mu L^{-1}$, Promega, C1181), 2 μL 0.1 M DTT, 4 μL 5× first strand buffer, 1 μL M-MLV Reverse Transcriptase (RT) (200 U $\mu L^{-1}$, Invitrogen, 28025-013, Breda, the Netherlands) and supplemented with RNAse-free ultra-pure water ($ddH_2O$). Genomic DNA contamination was checked with glyceraldehydes-3-phosphate dehydrogenase (GAPDH) primers, conventional PCR, and gel electrophoresis.

qPCR was executed to investigate the expression of genes related to cell phenotype, tissue formation, remodeling and ROS and enzyme production (Table 1) utilizing the primer sequences listed in ESI Table 1.† CYC-1 (macrophages) and GAPDH and B2M (the geometric mean, HVSCs) were used as reference genes. Expression was investigated by adding 1000 nM (CYC-1, GAPDH, B2M) or 500 nM primer mix (others), 5 μL SYBR Green Supermix (Bio-Rad; 170-8886), and an additional 1.75 μL $ddH_2O$ to 3 μL of diluted cDNA (10× diluted for the macrophages and 100× diluted for the HVSCs). $C_t$ values were acquired by exposing the mixtures to the following thermal protocol: 95 °C (3 min), 40 cycles of 95 °C (20 s), 60 °C (20 s), and 72 °C (30 s), 95 °C (1 min), and 65 °C (1 min), concluded with a melting curve measurement. Differences in expression profiles were determined by normalizing the $C_t$ values for the reference gene(s) ($\Delta C_t$), correcting these values for the $C_t$ value of the control ($\Delta\Delta C_t$) and applying the $2^{-\Delta\Delta Ct}$ formula to determine the fold changes in expression.

**2.4.4 Protein quantification: ELISA.** The protein secretion profiles of the stimulated macrophages were determined at day 4 and 8 (Table 1) using a multiplex immunoassay that relies on the Luminex technology (Multiplex core facility of the laboratory for Translational Immunology, UMC Utrecht, the Netherlands). The supernatants were incubated with antibody-conjugated MagPlex microspheres, followed by one hour incubation with biotinylated antibodies and an additional 10 minutes incubation with high performance ELISA (HPE) buffer diluted phycoerythrin-conjugated streptavidin. A

Table 1 Genes and proteins analysed *via* qPCR and multiplex ELISA

| Protein | Symbol | Function | qPCR | ELISA |
|---|---|---|---|---|
| **Phenotypic markers** | | | | |
| Cluster of differentiation 68 | CD68 | Pan-macrophage marker | x | |
| Monocyte chemoattractant protein 1 | MCP-1 | Chemotactic for monocytes/macrophages | x | x |
| Chemokine (C–C motif) receptor 7 | CCR7 | Pro-inflammatory macrophage marker | x | |
| Tumor necrosis factor alpha | TNF-α | Pro-inflammatory factor, stimulus for collagen production, inhibitor of elastogenesis | x | x |
| Interleukin 6 | IL-6 | Pro-inflammatory factor | | x |
| Mannose receptor c, type 1 | CD206 (MRC-1) | Anti-inflammatory macrophage marker | x | |
| Cluster of differentiation 163 | CD163 | Anti-inflammatory macrophage marker | x | |
| Interleukin 10 | IL-10 | Anti-inflammatory cytokine, inhibitor of collagen production | x | x |
| Interleukin 13 | IL-13 | Anti-inflammatory factor, stimulus for collagen production | | x |
| Transforming growth factor beta[a] | TGF-β | Anti-inflammatory factor; stimulus for collagen formation | x | x |
| Alpha smooth muscle actin | ACTA2 | Filament of the cytoskeleton involved in regulating cell shape, movement and involved in cell contractility | x | |
| Smoothelin | SMTN | Constitutes part of the cytoskeleton and is found exclusively in contractile smooth muscle cells | x | |
| Calponin | CNN1 | Protein that is involved in the modulation and regulation of smooth muscle cell contraction | x | |
| Vimentin | VIM | Intermediate filament protein, part of the cytoskeleton, fibroblast marker | x | |
| **Tissue formation** | | | | |
| Platelet derived growth factor-subunit BB | PDGF-BB | Stimulus for collagen formation and cell proliferation | | x |
| Connective tissue growth factor | CTGF | Stimulus for collagen formation | | x |
| Collagen type I | COL1A1 | Main structural load bearing protein of the extracellular matrix; most abundant collagen type. | x | |
| Collagen type III | COL3A1 | A fibrillar collagen; found frequently in association with type I collagen. | x | |
| Lysyl oxidase | LOX | Enzyme involved in collagen and elastin crosslinking | x | |
| Elastin | ELN | Tropoelastin, one of the main components of the elastic fiber | x | |
| Fibrillin-1 | FBN1 | Extracellular matrix protein that provides structural support for elastic fibril formation | x | |
| Fibrillin-2 | FBN2 | Extracellular matrix protein that provides structural support for elastic fibril formation | x | |
| Decorin | DCN | Proteoglycan important in collagen fibril assembly | x | |
| Versican | VCAN | Proteoglycan important for cell adhesion, proliferation, differentiation and migration. Proven important for elastic network formation | x | |
| **Remodeling** | | | | |
| Matrix metalloproteinase 1 | MMP-1 | ECM breakdown and remodeling | x | x |
| Matrix metalloproteinase 2 | MMP-2 | ECM breakdown and remodeling | x | |
| Matrix metalloproteinase 9 | MMP-9 | Anti-inflammatory factor involved in extra-cellular breakdown and remodeling | | x |
| Metallopeptidase inhibitor 1 | TIMP-1 | Inhibitor of MMP's | x | |
| Metallopeptidase inhibitor 2 | TIMP-2 | Inhibitor of MMP's | x | |
| **ROS and enzyme production** | | | | |
| Nicotinamide adenine dinucleotide phosphate-oxidase 2 | NOX2 | Enzyme complex that contributes to ROS production | x | |
| Nuclear factor kappa-light-chain-enhancer of activated B cells | NFKB1 | Involved in cellular responses to oxidative stress and cell survival | x | |
| Lipase A or cholesterol ester hydrolase | LIPA | Lysosomal enzyme | x | |

[a] The inactive protein latency-associated peptide-transforming growth factor-beta (LAP/TGF-β) was quantified *via* ELISA.

FLEXMAP 3D system with xPONENT 4.1 software (Luminex, Austin, TX) was used for data collection. Data was analysed by fitting a 5-parametric curve (Bio-PlexManager software, version 6.1.1, Biorad). The protein concentrations were corrected for medium evaporation and normalized to the average DNA content per experimental group. To determine the M1/M2 ratio, according to a previously reported method,[37] we calculated per cytokine the percentages of secretion in comparison to the mean secretion of the groups, followed by a division of the mean percentage of detected M1 cytokines (*i.e.*, IL-6, TNF-α, MCP-1) by the mean percentage of detected M2 cytokines (*i.e.*, IL-10, IL-13, MMP-9) per sample at day 8.

**2.4.5 Cell proliferation and nuclear integrity: immunohistochemistry.** Whole-mount samples of day 4 (HVSCs) and day 8 (macrophages and HVSCs) were stained for Ki67 and DAPI to evaluate cell proliferation and nuclear integrity. Formalin-fixed samples were washed in PBS and permeabilized (0.5% Triton-X 100 in PBS, 30 min), after which non-specific binding was

 

blocked using 5% (v/v) goat serum in a PBS solution containing 1% (w/v) bovine serum albumin (BSA, 30 min). The primary antibody Ki67 rabbit IgG (1 : 200, ThermoScientific) was diluted in a 10× diluted blocking solution and incubated overnight at 4 °C. After a PBS washing step (3 × 5 min), the fluorescently labeled secondary antibody goat anti-rabbit IgG-488 (1 : 500, Molecular Probes) was diluted in 10× diluted blocking solution and incubated for one hour at room temperature, simultaneously with 4′,6-diamidino-2-phenylindole (DAPI, 1 : 500, Sigma) to stain the cell nuclei. Whole-mounts were kept in PBS and visualized with a confocal laser scanning microscope (Leica TCS SP5X with a 63×/1.1 HCX PL Apo CS lens).

**2.4.6 Macrophage morphology and biomaterial degradation: SEM.** Prior to scanning electron microscopy (SEM), formaldehyde-fixed macrophage samples were dehydrated in ordered ethanol (EtOH) dilutions (50% EtOH to 100% EtOH in steps of 10%) and dried in vacuum overnight. Samples were imaged with SEM at representative locations (magnifications 50×, 500×, 1500× and 2500×) as described in section 2.2. After visualization, the samples were decellularized with 4.6% sodium hypochlorite for 15 minutes at room temperature followed by two washing steps (2 × 5 min $H_2O$). The decellularized samples were gold-sputtered, together with the cell-free samples, and visualized using SEM (high vacuum, 10 kV electron beam) to evaluate scaffold degradation.

**2.4.7 Scaffold mass loss.** To further quantify biomaterial degradation, decellularized macrophage samples and cell-free samples were weighed using a digital balance. Obtained weights were corrected for the measured surface area. To determine the remaining mass fraction, the remaining mass per $mm^2$ was normalized to the initial mass per $mm^2$.

**2.4.8 Scaffold melting curves: DSC.** Prior to analysis, cell-free samples were weighed, transferred to Tzero aluminium pans and hermetically sealed. Differential scanning calorimetry (DSC) measurements were performed in a DSC Q2000 (TA instruments, USA). The samples were exposed to three heating/cooling cycles (−70 °C to 160 °C in a rate of 10 °C $min^{-1}$). Melting peaks (peak maxima) and melting enthalpies (surfaces under the peak) were calculated form the first heating run using Universal Analysis software (V4.5A, TA Instruments).

**2.4.9 Scaffold molecular weight: GPC.** After lyophilization, cell-free samples reserved for gel permeation chromatography (GPC), were dissolved in dimethylformamide, supplemented with 10 mM LiBr and 0.25% (v/v) $H_2O$, at a concentration of 1 mg $mL^{-1}$, and filtered using a 0.2 μm regenerated cellulose filter. A Varian/Polymer Laboratories PL-GPC 50 Plus instrument (Varian Inc., Palo Alto, CA, USA) operated at 50 °C, equipped with a Shodex GPC KD-804 column (Shodex, Tokyo, Japan) was used to determine the weight- and number-averaged molecular weights ($M_w$ and $M_n$) relative to poly(ethylene glycol) standards.

### 2.5 Statistical analyses

All data are presented either as the mean ± standard deviation or as boxplots. Obtained qPCR data were logarithmically transformed before statistical analysis. Since the data was not normally distributed according to the Shapiro–Wilk test, the non-parametric Kruskal–Wallis test with a Dunn's multiple comparison test were performed to identify statistically significant differences (GraphPad, La Jolla, CA, USA) between the experimental groups. Differences were considered as statistically significant for $p$-values below 0.05.

## 3. Results and discussion

### 3.1 Characterization of scaffolds and hemodynamic loads

Tubular PCL-BU scaffolds were created with an inner diameter of 3 mm and a wall thickness of approximately 200 μm. The scaffolds exhibited a porous isotropic microstructure with an average fiber diameter of 5.0 ± 0.5 μm and pore size of 8.6 ± 3.2 $\mu m^2$. The macrophage-seeded scaffolds were cultured in the bioreactor that imposed physiological loading on the constructs with an average of 3.7 ± 0.8% strain (~1.04 stretch) and/or 1.2 ± 0.1 Pa wall shear stress (ESI Fig. S2†).

### 3.2 Hemodynamic loading does not affect scaffold physicochemical integrity

Cell-free experiments were performed for 8 days to investigate if physiological mechanical loading alone changed the physical and chemical properties of the material (Fig. 1A). SEM analysis revealed no differences between the fiber morphologies and organizations in the various experimental groups and the bare scaffold control (Fig. 1B, Table 2 and ESI Fig. S2†). Consistent with this, no reductions or inequalities in sample mass were detected between the experimental groups (Table 2). We detected a small increase in overall scaffold mass for all cell-free experimental samples after 8 days culture in comparison to the bare scaffold control (Table 2), which could be attributed to absorption of medium components during the course of the experiment.

In terms of the polymer molecular weight, minor differences were detected as a consequence of culture or loading (Table 2). DSC measurements showed comparable crystalline melt transitions at approximately 15 °C and 120 °C and minor differences in recorded melting enthalpies for the soft PCL and hard bis-urea blocks, respectively. In addition, a second PCL melting peak was detected around 50 °C, presumably as a consequence of the electrospinning process, with variations in recorded enthalpies that could indicate that there are minor differences in crystallinity between the experimental groups. These differences in crystallinity seem, however, unrelated to either culture or loading conditions (Fig. 1C and Table 2).

### 3.3 Hemodynamic loads differentially affect macrophage number and distribution throughout the scaffold

A previous *in vivo* study showed that both tissue formation and scaffold degradation are highly heterogeneous and dependent on the amount and type of infiltrating immune cells.[30] Herein, we hypothesized that biomechanical loading plays a large part, as loading has been shown to impact cell attachment as well

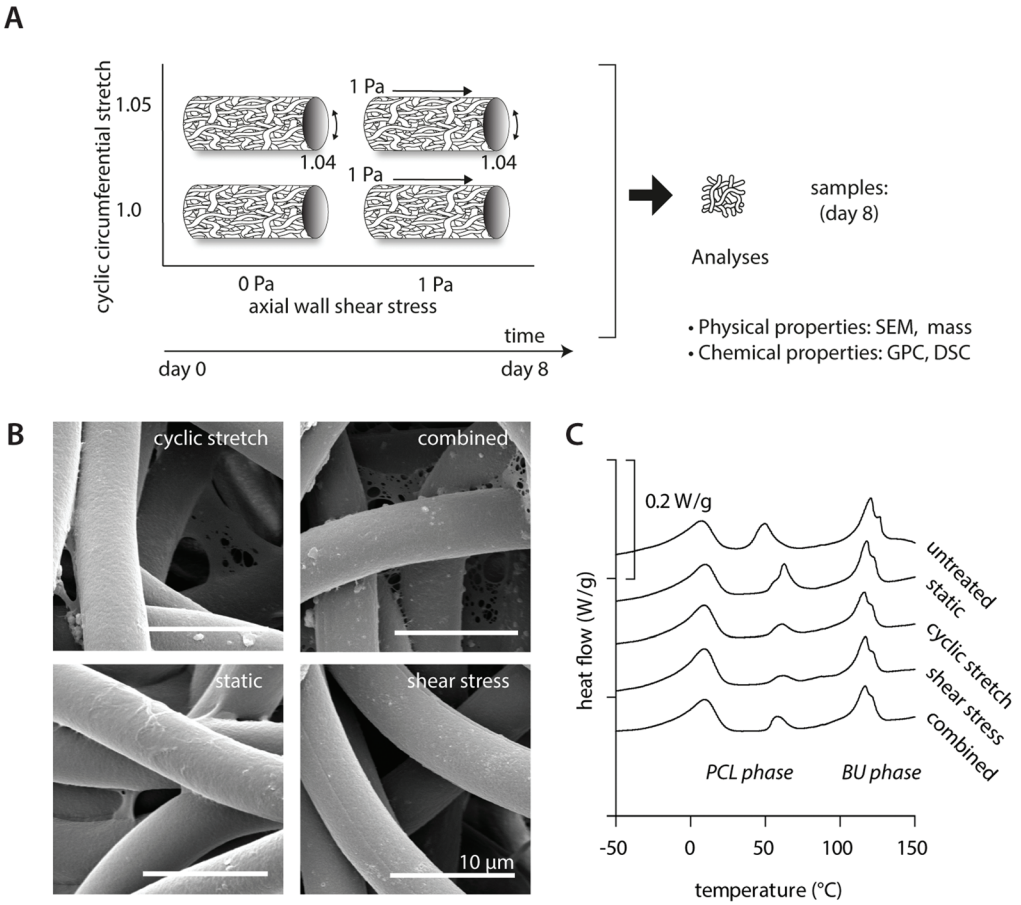


**Fig. 1** Scaffold characterization of the cell-free scaffolds at day 8. Lay-out of the study design of the cell-free experiments (A); SEM images showing the fiber morphology and fibrin remnants for the different experimental groups (B); representative DSC curves (in arbitrary order) for each experimental group in comparison to an untreated control (C).

as cell apoptosis.[24,25,38,39] To investigate the consequences of hemodynamic loading on macrophage number and distribution, THP-1 derived macrophages were cultured for 8 days on tubular scaffolds under comparable physiological loading conditions as used for the cell-free experiments (Fig. 2A).

Overall, cell seeding resulted in cellular infiltration and distribution throughout the complete scaffold thickness. After 8 days of culture, macrophages reduced in number and adopted a flattened morphology, following and covering the scaffold microarchitecture (Fig. 2B and C). The statically cultured samples demonstrated a more homogeneous cellular distribution throughout the whole scaffold compared to the hemodynamically loaded samples. Mechanically loaded macrophages predominantly resided at the loci of seeding during the course of the experiment, suggesting that mechanical loading reduces cellular migration. This decrease in migration might be explained by a potential increase in macrophage intracellular tension upon loading, as it is seen that macrophage migratory speed is inversely correlated to the intracellular tension.[40,41]

Besides the overall migratory capacity, cell attachment and apoptosis will determine the distribution and density within the construct, which can be modulated by mechanical loads.[24,38,39] For example, Shive *et al.* demonstrated that both material surface and increasing shear flow affect monocyte apoptosis.[25] In the present study, SEM analysis and DNA quantification revealed a reduction in the overall cell number for the shear stress samples in comparison to the statically cultured controls (0.7 ± 0.2 µg *vs.* 1.0 ± 0.4 µg DNA per mg scaffold), especially in the superficial scaffold layers (Fig. 2B and C). Although cellular integrity might be affected by exposure to shear stress, potentially resulting in DNA fragmentation, we observed predominantly intact cell nuclei with no differences between the experimental groups (Fig. 2D). Therefore, we reasoned that the superficial cells were flushed away during the course of the experiment. Surprisingly, these reductions in cellular content were partially negated when cyclic stretch was simultaneously applied (both loads combined: 0.9 ± 0.3 µg DNA per mg scaffold). In line with this observation, we detected the highest cellular contents for the cyclically stretches samples (1.3 ± 0.4 µg DNA per mg scaffold). These findings suggest that cyclic stretch ameliorated cellular attachment and/or induced proliferation (Fig. 2B). Although the occurrence of macrophage proliferation is not frequently

 

**Table 2** Remaining mass, fiber diameter and chemical properties as measured by GPC and DSC of the cell-free samples at day 8

| | | Condition | | | | |
|---|---|---|---|---|---|---|
| Degradation read-out | | Static | Cyclic stretch | Shear stress | Combined | Untreated |
| Mass | Remaining mass (–) | 1.23 ± 0.07 | 1.21 ± 0.04 | 1.22 ± 0.07 | 1.28 ± 0.13 | 1 |
| SEM | Fiber diameter (μm) | 5.2 ± 0.2 | 5.1 ± 0.2 | 5.1 ± 0.2 | 5.1 ± 0.2 | 5.0 ± 0.5 |
| GPC | $M_w$ (kg mol$^{-1}$) | 29.8 ± 3.6 | 31.9 ± 3.3 | 31.4 ± 4.1 | 30.6 ± 3.5 | 33.7 ± 3.8 |
| | $M_n$ (kg mol$^{-1}$) | 16.8 ± 2.2 | 18.4 ± 2.3 | 17.8 ± 2.0 | 17.8 ± 2.0 | 18.9 ± 2.2 |
| | PDI ($M_w/M_n$) | 1.78 ± 0.09 | 1.74 ± 0.06 | 1.76 ± 0.08 | 1.72 ± 0.10 | 1.78 ± 0.01 |
| DSC | Melting enthalpy (J g$^{-1}$) | | | | | |
| | PCL phase | 5.95 ± 4.49 | 3.44 ± 0.41 | 4.07 ± 0.77 | 4.58 ± 1.67 | 4.71 ± 2.60 |
| | BU phase | 7.97 ± 1.41 | 8.62 ± 0.54 | 8.42 ± 0.88 | 8.78 ± 0.25 | 8.28 ± 1.92 |
| | Melting temperature (°C) | | | | | |
| | PCL phase | 63 ± 1 | 61 ± 1 | 61 ± 2 | 61 ± 2 | 53 ± 2 |
| | BU phase | 118 ± 1 | 117 ± 1 | 118 ± 1 | 117 ± 1 | 121 ± 1 |

Abbreviations: scanning electron microscopy (SEM), gel permeation chromatography (GPC), weight ($M_w$) and number ($M_n$) averaged molecular weights, polydispersity index (PDI) and differential scanning calorimetry (DSC).

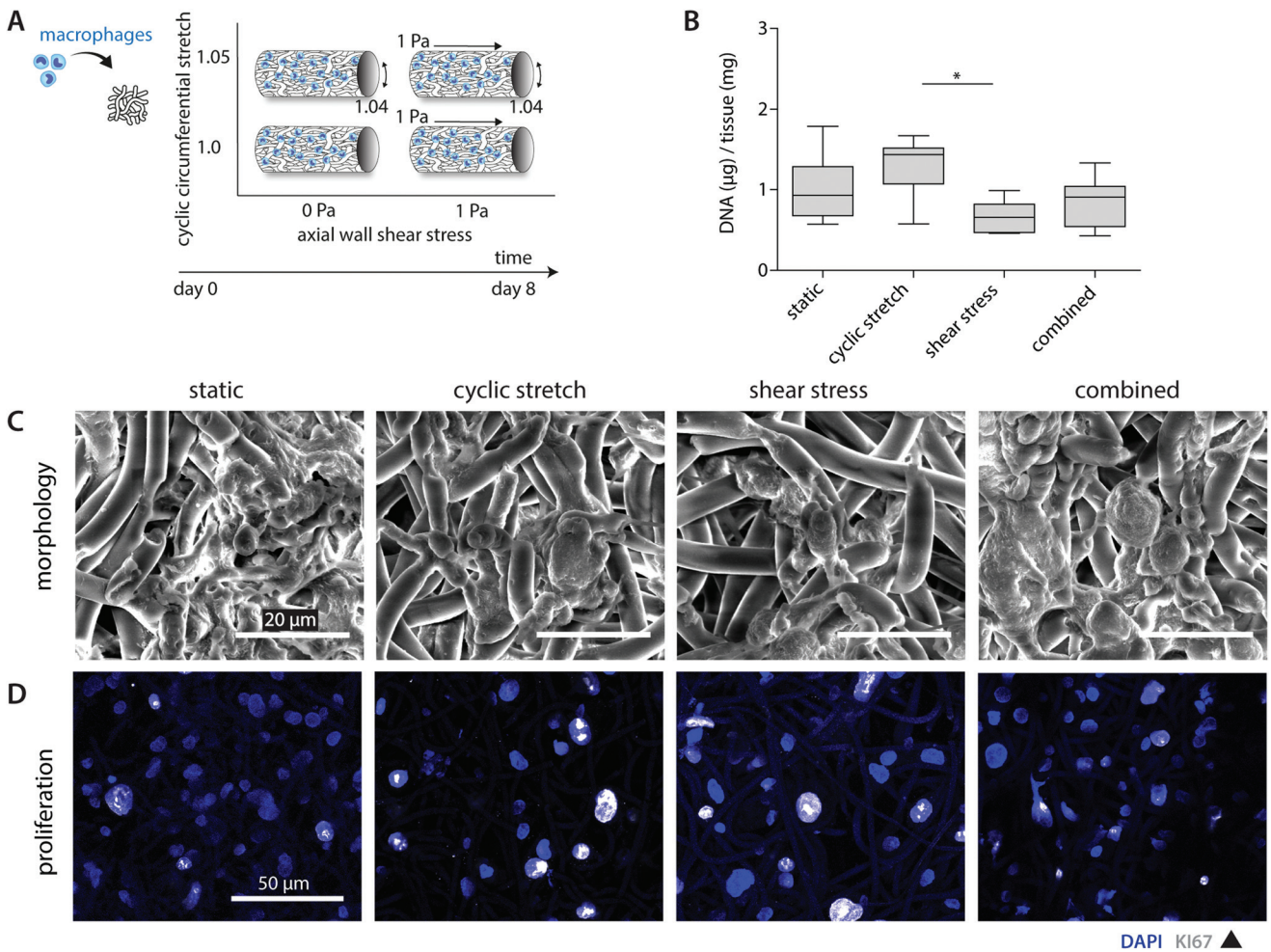


**Fig. 2** Macrophage number, morphology and proliferative state after 8 days of culture. Lay-out of the study design (A); DNA content per experimental group at day 8 ($n$ = 5 or 6 per group) normalized to the construct mass (* $p < 0.05$) (B); representative SEM images showing the cell morphology of the statically and dynamically cultured macrophages (C); representative pictures of the Ki67 and DAPI staining visualizing the proliferating macrophages (whole mount staining, overlay of $z$-stack ± 25 μm, blue = DAPI; white = Ki67) (D).

described, a recent study pointed out that rapid *in situ* proliferation of macrophages might occur in order to increase population density.[42] Indeed, Ki67 positive proliferating macrophages were observed within our experiments (Fig. 2D). However, no differences were seen between the loading regimes applied. Altogether, these results confirm that mechanical loading affects cellular number and distribution.

### 3.4 Macrophage phenotype depends on hemodynamic loads applied

The mechanoregulation of macrophage phenotype and behaviour is increasingly acknowledged but still poorly understood.[29] Recent studies highlighted that low and oscillatory flow patterns could stimulate a more pro-inflammatory profile in macrophages *in vivo*.[43,44] Moreover, moderate levels of cyclic strain (~8%) have been shown *in vitro* to promote a more reparative macrophage phenotype and cytokine secretion profile in comparison to higher strain levels (≥12%).[28,45] To examine macrophage polarization for the various physiological loading regimes applied, we compared the gene expression and protein secretion profiles in our constructs (Fig. 3, 4 and ESI Fig. S3, S4†).

Exposure to mechanical loading resulted in clear and significant increases in pro-inflammatory MCP1, TNF and anti-inflammatory IL10 gene expression when compared to the statically cultured controls, especially in conditions of shear stress (MCP1) and cyclic stretch (TNF and IL10) (Fig. 3A). In contrast, a decrease in pro-inflammatory CCR7 gene expression was detected upon mechanical loading, which was significantly different and most pronounced in the presence of shear stress. CCR7 was initially described as a potent chemotactic receptor expressed by migrating leukocytes,[46–48] like macrophages, substantiating our hypothesis that mechanical loading reduces cellular migration. In addition, several recent studies have highlighted the importance of CCR7 in the control over cell survival, cell cytoskeleton turnover, the rate of endocytosis, and the migratory speed of leukocytes.[49–51] Furthermore, minor and non-significant increases in anti-inflammatory CD163 and CD206 gene expression were seen when macrophages were mechanically loaded, and no differences were detected for TGFB1, MMP9 and pan-macrophage CD68 gene expression (Fig. 3B).

At the protein level, similar trends were observed, albeit with some variations (Fig. 4 and ESI Fig. S4, S5†). Again, elevated levels of MCP-1 and IL-10 secretion were measured upon hemodynamic loading (Fig. 4A). For these cytokines, significantly higher secretion levels were detected for those samples that were exposed to both loads simultaneously when compared to the statically cultured controls. Similarly, the highest levels of IL-6, TNF-α, and PDGF-BB were detected when both loads were combined when compared to the individual loads or no loading at all (Fig. 4B). On the other hand, TGF-β secretion, measured as the inactive form LAP/TGF-β, was clearly inhibited upon mechanical loading, while negligible differences between the experimental groups were found for CTGF (Fig. 4A and B). The reduction in measured LAP/TGF-β for the dynamically cultured experimental groups might be caused by the mechanical disruption of the non-covalent binding between LAP and TGF-β, activating the protein and making the protein undetectable by ELISA.[52] With respect to ECM remodeling, as evaluated by MMP-1 and MMP-9 secretion, high levels of proteins were measured, regardless of the presence or type of load (Fig. 4B). Lastly, a minor upregulation of anti-inflammatory IL-13 secretion was detected in the presence of cyclic stretch (Fig. 4B).

The calculated M1/M2 ratios, which were determined based on the secretion levels of the pro- and anti-inflammatory cytokines, demonstrate a moderate increase upon mechanical loading with the highest ratio detected if both shear stress and cyclic stretch are combined (Fig. 4C).

Overall, these data expose that physiological loading conditions stimulate macrophage activation, especially when both loads are combined, and contribute to a mixed macrophage phenotype that varies in its gene expression and protein secretion profile dependent on the loading protocol applied.

### 3.5 Cyclic stretch decreases macrophage-driven biomaterial degradation

To better determine macrophage behavior and scaffold performance, scaffolds were decellularized to assess biomaterial degradation. After 8 days of culture, clear fiber erosion, cleavage and mass loss were detected in all experimental groups, as demonstrated by SEM analysis and the remaining scaffold mass (Fig. 5A and B). The highest percentages of degradation were seen for the statically cultured samples, while the shear stress samples remained most intact. When corrected for the DNA content, a significantly lower degradation capacity was detected for the cyclically stretched macrophages in comparison to the static control (Fig. 5B). Similarly, we observe minor but significant reductions in the average MDA levels upon cyclic stretching when compared to the static control, suggesting a tendency for reduced oxidative degradation (Fig. 5C). In line with these observations, Patel *et al.* demonstrated that substrate stretch resulted in reductions in cellular elasticity, inhibiting the ROS secretion and the phagocytosis capacity of murine macrophages.[53] As cell-free samples were not affected after hemodynamic loading (Fig. 1), we speculate that reduced cellular elasticity as a result of cyclic stretch may have played a role in the reductions in the degradative capacity of the macrophage (*i.e.* reduced scaffold mass loss). However, at the gene level, no significant differences were seen in the expression of NOX2, NFKB1 or LIPA (Fig. 5C).

### 3.6 Mechanically conditioned macrophages distinctly regulate (myo)fibroblast behaviour *via* paracrine signalling

Besides their degradative potential, macrophages are known for their role as mediators in tissue formation and remodeling.[1,54] *Via* paracrine signaling, M2 macrophages have been shown to stimulate fibroblast proliferation and subsequent collagen deposition, while a more pro-inflammatory M1 macrophage profile augments the tissue degradative potential.[5,14,55–57]

 

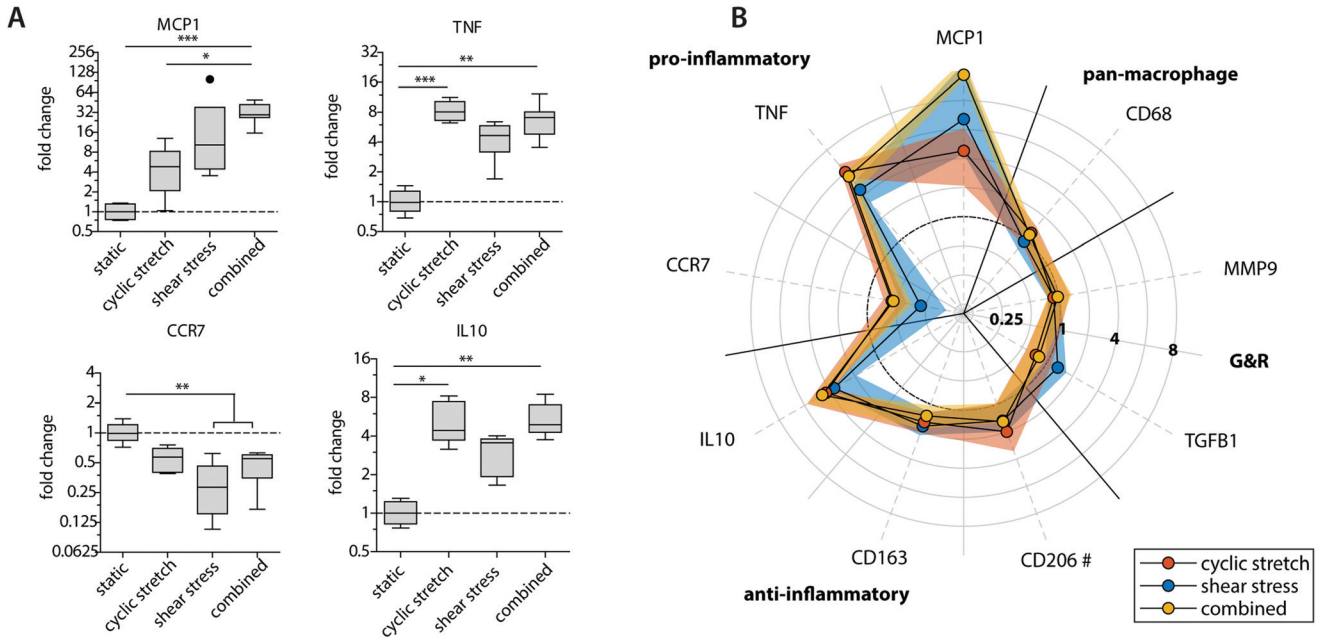


**Fig. 3** Gene expression profiles of the statically and dynamically cultured macrophages at day 8. Boxplots representing the fold changes in relative gene expression for a selection of phenotypical-related genes. The dot represents a statistical outlier (A); graphical representation of the fold changes in relative gene expression of the pan-macrophage marker CD68, pro- and anti-inflammatory markers, as well as markers related to growth and remodeling (G&R) when compared to the statically cultured control. The dots and shaded areas indicate, respectively, the 50th and 25th–75th percentiles (B). * $p < 0.05$; ** $p < 0.01$; *** $p < 0.001$. $n \geq 5$ per group. # $n \geq 2$ per group.

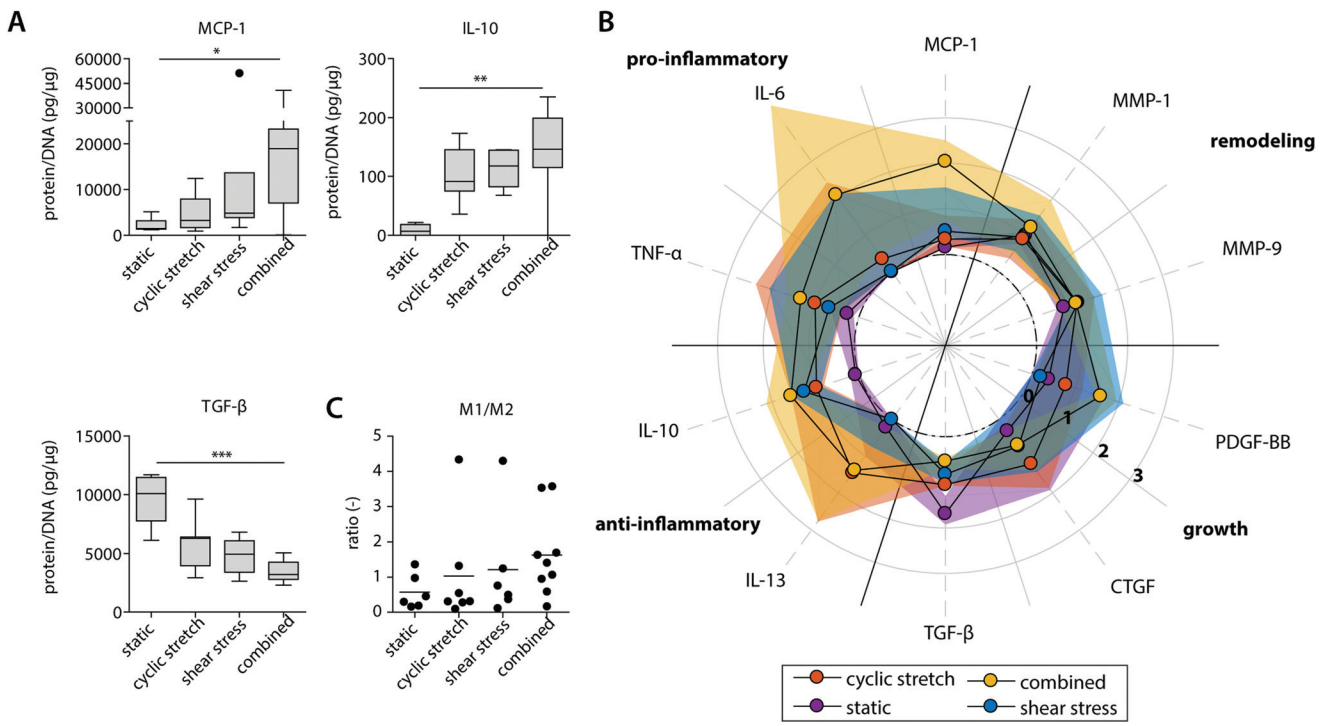


**Fig. 4** Protein secretion profiles of the statically and dynamically cultured macrophages at day 8. Boxplots visualizing the secretion levels of a selection of proteins. The dot represents a statistical outlier (A); relative secretion levels compared to the average secretion of pro-inflammatory, anti-inflammatory, growth and remodeling proteins (protein levels were corrected for the average DNA content per group). The dots and shaded areas indicate, respectively, the 50th and 25th–75th percentiles (B); calculated M1/M2 ratios based on the cytokine secretion levels of IL-6, TNF-α, MCP-1 (pro-inflammatory) and IL-10, IL-13, MMP-9 (anti-inflammatory) (C). * $p < 0.05$; ** $p < 0.01$, *** $p < 0.001$. $n \geq 5$ per group per time point. See ESI Fig. S5† for the uncorrected data at day 4 and 8.

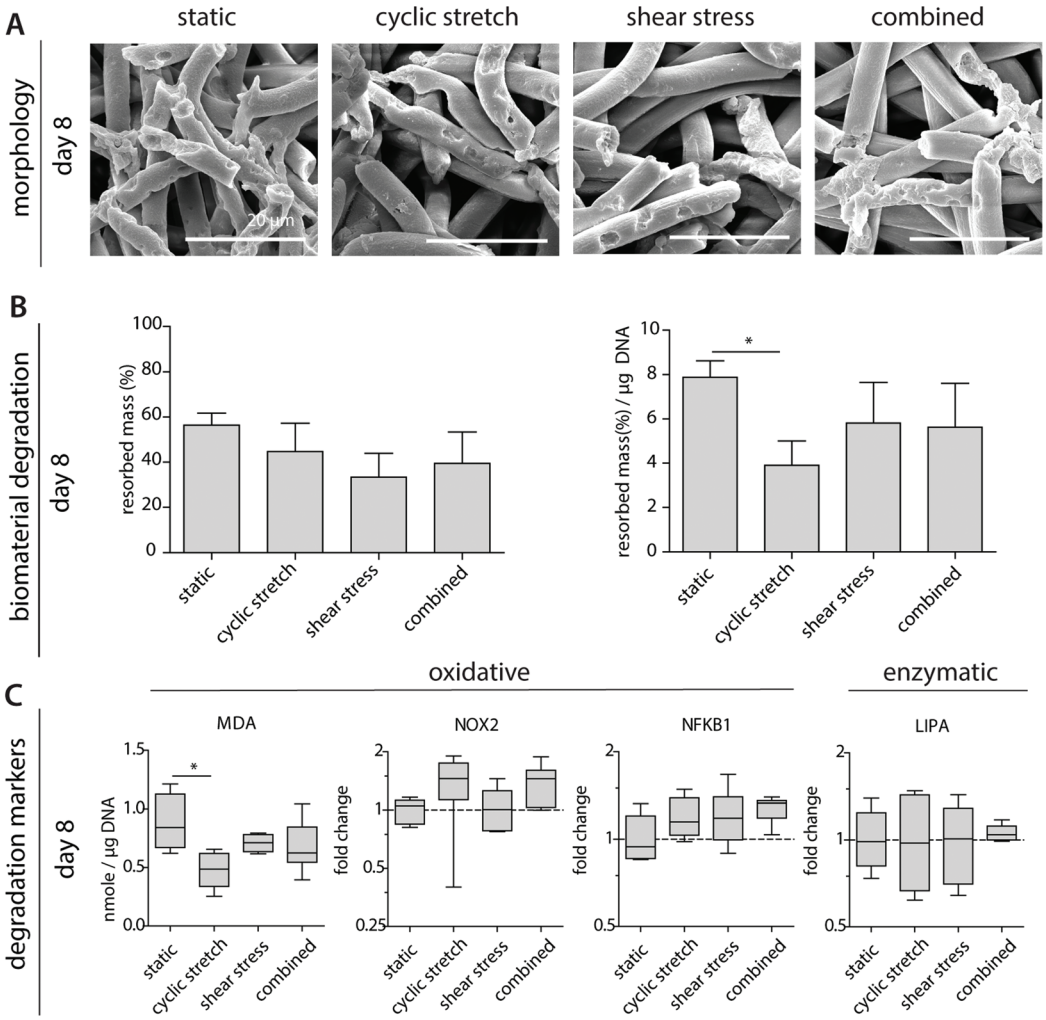


**Fig. 5** Macrophage-driven biomaterial degradation. Representative SEM images of decellularized samples after 8 days of culture (A); calculated average percentages of overall mass resorption and mass resorption normalized to DNA content, $n \geq 3$ per group (B); oxidative and enzymatic degradation markers including malondialdehyde (MDA) presence, as an indirect measure of oxidative degradation, and the expression of the oxidative genes NOX-2 (ROS generating NADPH Oxidase 2 complex), NFKB1 (protein complex involved in oxidative stress) or LIPA (lysosomal lipase) (compared to CYC-1) at day 8. * $p < 0.05$, $n \geq 5$ per group per time point.

We assessed the paracrine effects of our dynamically cultured macrophages on scaffold-seeded (myo)fibroblasts and observed minor differences in the proliferation or number of (myo)fibroblasts between the experimental groups (see ESI Fig. S6†). The macrophage-conditioned media resulted in clear alterations in the gene expression profiles of the (myo)-fibroblasts, which became most apparent after 8 days of paracrine stimulation (Fig. 6 and ESI Fig. S7†). The phenotypic markers SMTN and VIM were enhanced in (myo)fibroblasts that were exposed to the paracrine factors of shear stress and cyclic stretch-stimulated macrophages (Fig. 6A). The contractile markers ACTA2 and CNN1 exhibited an opposite pattern. Predominantly ACTA2 demonstrated a decrease in expression when exposed to the supernatants of the mechanically loaded macrophages, which was significantly lowest in the shear stress group. With respect to tissue deposition and remodeling, we detected only minor differences in gene expressions for the HVSCs that were exposed to cyclically stretched macrophage-conditioned medium compared to the static controls (Fig. 6B). On the contrary, ECM-related gene expression patterns tended to increase for those HVSCs that were exposed to the supernatants of the shear stress-stimulated macrophages, and especially when combined with cyclic stretch. More specifically, significantly higher COL3A1, VCAN, and TGFB1 expressions were seen for the combined group in comparison to the static control and/or the cyclic stretch group (Fig. 6C). Similar trends were observed for IL6, DCN, and ELN, however differences were minor. On the contrary, we detected a simultaneous reduction in FBN1 and FBN2 expressions, which code for microfibrillar proteins that are essential for functional elastic network formation (Fig. 6B).[58]

 

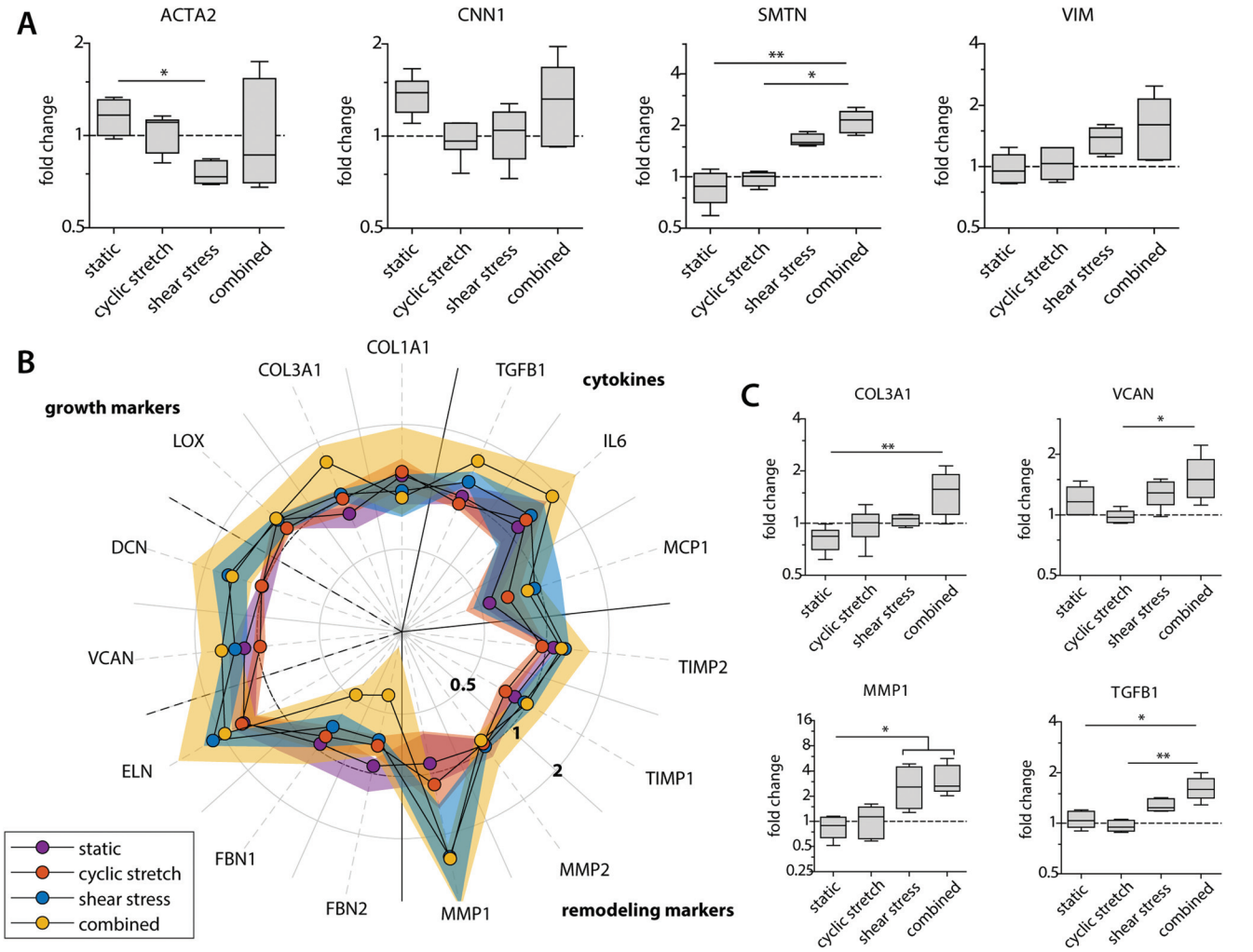


Fig. 6 Gene expression profiles of the HVSCs at day 8. Boxplots visualizing the fold changes in relative expression of the (myo)fibroblast phenotypical markers (A); and markers related to collagen, GAGs/proteoglycans and elastic matrix deposition or matrix remodeling (C) in comparison to the (myo)fibroblast samples that were cultured in fresh medium (control); fold changes in gene expression compared to the control for genes related to collagen matrix, GAGs/proteoglycans, and elastic matrix formation (left part of the polar plot), as well as markers related to remodeling and cytokine secretion (right part of the polar plot). The dots and shaded areas indicate, respectively, the 50th and 25th–75th percentiles (B). * $p < 0.05$; ** $p < 0.01$. $n \geq 5$ per group.

Importantly, shear stress not only upregulated fibrogenic genes but also stimulated an increase in the expression of genes related to ECM-remodeling in the (myo)fibroblasts (*i.e.* MMP1, TIMP1 and 2), suggesting that macrophage signaling may contribute to functional tissue deposition and remodeling, rather than purely stimulating fibrotic tissue formation (Fig. 6B and C). While it is well-established that hemodynamic stimuli have a direct effect on the fibrogenic potency of (myo)-fibroblast-like cells, both in terms of cyclic stretch[59–62] and, to a less extent, shear stress,[63] our findings reveal an important paracrine route by which hemodynamic loads affect ECM formation and remodeling by (myo)fibroblasts. These paracrine effects were most evident in the presence of shear stress and most pronounced in the combined conditions of both shear stress and cyclic stretch, but limited to negligible in the presence of cyclic stretch only.

## 4. Limitations of the study

In the present study, we opted for human THP1 cell-line derived macrophages over primary human macrophages in order to be able to obtain sufficient cell numbers to account for all experimental conditions and avoid large donor-to-donor variabilities. Despite the fact that the polarization profile of cyclically stretched THP-1 cell-line derived macrophages largely matches with the primary variant,[28,45] it is known that THP-1 macrophages can deviate from primary cells in their cytokine secretion profile.[64] Moreover, scaffold degradation is dependent on the interactions of multiple phagocytes (*e.g.* monocytes and neutrophils) and interrelated degradation pathways.[10,65,66] Other cells might pretreat the material with their degradative compounds, changing the material's susceptibility to degrade.[65,67] This study did not account for potential

variations in the resident cell populations, mutual cell communication and the spatio-temporal differences in loading as a consequence of degradation and tissue deposition. Furthermore, we only evaluated the early macrophage response. It is interesting to prolong these experiments in the future to investigate how the differences in scaffold degradation and tissue formation between the experimental groups will develop over time.

## 5. Conclusions

This study reveals for the first time the individual and combined effects of physiological shear stress and cyclic stretch on macrophage polarization and macrophage-driven *in vitro* vascular tissue regeneration. These results provide novel insights into the effect of mechanical cues and cell–cell interplay during the early stages of *in situ* tissue development and underline the importance of considering the potential spatio-temporal variations in cyclic stretch and shear stress when designing scaffolds for *in situ* vascular tissue engineering. Future work should focus on the local hemodynamic loads sensed by the cells within the scaffold, the underlying mechanisms of the mechanoresponse and the effects of loading on later stage biomaterial degradation and tissue development to adequately tailor immunomodulatory scaffold design.

## Conflicts of interest

There are no conflicts to declare.

## Acknowledgements

The authors would like to thank Marina van Doeselaar for her assistance in the sample analysis. This study is financially supported by ZonMw as part of the LSH 2Treat program (436001003) and the Dutch Kidney Foundation (14a2d507). We gratefully acknowledge the Gravitation Program "Materials Driven Regeneration", funded by the Netherlands Organization for Scientific Research (024.003.013).

## References

1 T. B. Wissing, V. Bonito, C. V. C. Bouten and A. I. P. M. Smits, Biomaterial-driven in situ cardiovascular tissue engineering—a multi-disciplinary perspective, *npj Regener. Med.*, 2017, **2**(18), DOI: 10.1038/s41536-017-0023-2.

2 A. I. P. M. Smits and C. V. C. Bouten, Tissue Engineering meets Immunoengineering: Prospective on Personalized In Situ Tissue Engineering Strategies, *Curr. Opin. Biomed. Eng.*, 2018, **6**(March), 17–26, DOI: 10.1016/j.cobme.2018.02.006.

3 W. Kenneth Ward, A review of the foreign-body response to subcutaneously-implanted devices: the role of macrophages and cytokines in biofouling and fibrosis, *J. Diabetes Sci. Technol.*, 2008, **2**(5), 768–777, DOI: 10.1177/193229680800200504.

4 B. M. Delavary, W. M. van der Veer, M. van Egmond, F. B. Niessen and R. H. J. Beelen, Macrophages in skin injury and repair, *Immunobiology*, 2011, **216**(7), 753–762, DOI: 10.1016/j.imbio.2011.01.001.

5 D. T. A. Ploeger, N. A. Hosper, M. Schipper, J. A. Koerts, S. De Rond and R. A. Bank, Cell plasticity in wound healing : paracrine factors of M1/M2 polarized macrophages influence the phenotypical state of dermal fibroblasts, *Cell Commun. Signaling*, 2013, **11**(29), 1–17, DOI: 10.1186/1478-811X-11-29.

6 A. Mantovani, S. K. Biswas, M. R. Galdiero, A. Sica and M. Locati, Macrophage plasticity and polarization in tissue repair and remodelling, *J. Pathol.*, 2013, **229**(2), 176–185, DOI: 10.1002/path.4133.

7 A. Sica and A. Mantovani, Macrophage plasticity and polarization: in vivo veritas, *J. Clin. Invest.*, 2012, **122**(3), 787–795, DOI: 10.1172/JCI59643DS1.

8 L. Pastorino, F. Pioli, M. Zilli, A. Converti and C. Nicolini, Lipase-catalyzed degradation of poly(ε-caprolactone), *Enzyme Microb. Technol.*, 2004, **35**(4), 321–326, DOI: 10.1016/j.enzmictec.2004.05.005.

9 H. Peng, J. Ling, J. Liu, N. Zhu, X. Ni and Z. Shen, Controlled enzymatic degradation of poly(ε-caprolactone)-based copolymers in the presence of porcine pancreatic lipase, *Polym. Degrad. Stab.*, 2010, **95**(4), 643–650, DOI: 10.1016/j.polymdegradstab.2009.12.005.

10 J. E. McBane, J. P. Santerre and R. S. Labow, The interaction between hydrolytic and oxidative pathways in macrophage-mediated polyurethane degradation, *Clin. Exp. Rheumatol.*, 2007, **33**(4), 97–103, DOI: 10.1002/jbm.a.31263.

11 M. C. P. Brugmans, S. H. M. Söntjens, M. A. J. Cox, *et al.*, Hydrolytic and oxidative degradation of electrospun supramolecular biomaterials: In vitro degradation pathways, *Acta Biomater.*, 2015, **27**, 21–31, DOI: 10.1016/j.actbio.2015.08.034.

12 K. G. Battiston, R. S. Labow, C. A. Simmons and J. P. Santerre, Immunomodulatory polymeric scaffold enhances extracellular matrix production in cell co-cultures under dynamic mechanical stimulation, *Acta Biomater.*, 2015, **24**, 74–86, DOI: 10.1016/j.actbio.2015.05.038.

13 K. G. Battiston, B. Ouyang, R. S. Labow, C. A. Simmons and J. P. Santerre, Monocyte/macrophage cytokine activity regulates vascular smooth muscle cell function within a degradable polyurethane scaffold, *Acta Biomater.*, 2014, **10**(3), 1146–1155, DOI: 10.1016/j.actbio.2013.12.022.

14 E. Song, N. Ouyang, M. Hörbelt, B. Antus, M. Wang and M. S. Exton, Influence of Alternatively and Classically Activated Macrophages on Fibrogenic Activities of Human Fibroblasts, *Cell. Immunol.*, 2000, **204**(1), 19–28, DOI: 10.1006/cimm.2000.1687.

 

15 B. N. Brown, R. Londono, S. Tottey, *et al.*, Macrophage phenotype as a predictor of constructive remodeling following the implantation of biologically derived surgical mesh materials, *Acta Biomater.*, 2012, **8**(3), 978–987, DOI: 10.1016/j.actbio.2011.11.031.

16 T. Yu, W. Wang, S. Nassiri, *et al.*, Temporal and spatial distribution of macrophage phenotype markers in the foreign body response to glutaraldehyde- crosslinked gelatin hydrogels, *J. Biomater. Sci., Polym. Ed.*, 2016, **118**(24), 6072–6078, DOI: 10.1080/09205063.2016.1155881.

17 K. L. Spiller, S. Nassiri, C. E. Witherel, *et al.*, Sequential delivery of immunomodulatory cytokines to facilitate the M1-to-M2 transition of macrophages and enhance vascularization of bone scaffolds, *Biomaterials*, 2015, **37**, 194–207, DOI: 10.1016/j.biomaterials.2014.10.017.

18 E. E. van Haaften, R. Duijvelshoff, B. D. Ippel, *et al.*, The degradation and performance of electrospun supramolecular vascular scaffolds examined upon in vitro enzymatic exposure, *Acta Biomater.*, 2019, **92**(July), 48–59, DOI: 10.1016/j.actbio.2019.05.037.

19 S. Lyu and D. Untereker, Degradability of polymers for implantable biomedical devices, *Int. J. Mol. Sci.*, 2009, **10**(9), 4033–4065, DOI: 10.3390/ijms10094033.

20 B. D. Riehl, J.-H. Park, I. K. Kwon and J. Y. Lim, Mechanical Stretching for Tissue Engineering: Two-Dimensional and Three-Dimensional Constructs, *Tissue Eng., Part B*, 2012, **18**(4), 288–300, DOI: 10.1089/ten.teb.2011.0465.

21 E. E. Van Haaften, C. V. C. Bouten and N. A. Kurniawan, Vascular Mechanobiology : Towards Control of In Situ Regeneration, *Cells*, 2017, **6**(19), 1–24, DOI: 10.3390/cells6030019.

22 E. E. van Haaften, T. B. Wissing, M. Rutten, *et al.*, Decoupling the effect of shear stress and stretch on tissue growth & remodeling in a vascular graft, *Tissue Eng., Part C*, 2018, **24**(7), 418–429, DOI: 10.1089/ten.TEC.2018.0104.

23 Z. M. Ruggeri, Platelet adhesion under flow, *Microcirculation*, 2009, **16**(1), 58–83, DOI: 10.1080/10739680802651477.

24 S. Chen and T. A. Springer, Selectin receptor-ligand bonds: Formation limited by shear rate and dissociation governed by the Bell model, *Proc. Natl. Acad. Sci. U. S. A.*, 2001, **98**(3), 950–955, DOI: 10.1073/pnas.98.3.950.

25 M. S. Shive, W. G. Brodbeck, E. Colton and J. M. Anderson, Shear stress and material surface effects on adherent human monocyte apoptosis, *J. Biomed. Mater. Res.*, 2002, **60**(1), 148–158, DOI: 10.1002/jbm.10035.

26 J. H. Yang, H. Sakamoto, E. C. Xu and R. T. Lee, Biomechanical regulation of human monocyte/macrophage molecular function, *Am. J. Pathol.*, 2000, **156**(5), 1797–1804, DOI: 10.1016/S0002-9440(10)65051-1.

27 R. Ohki, K. Yamamoto, H. Mano, R. T. Lee, U. Ikeda and K. Shimada, Identification of mechanically induced genes in human monocytic cells by DNA microarrays, *J. Hypertens.*, 2002, **20**(4), 685–691, DOI: 10.1097/00004872-200204000-00026.

28 V. Bonito, B. J. de Kort, C. V. C. Bouten and A. I. P. M. Smits, Cyclic Strain affects Macrophage Cytokine Secretion and ECM turnover in Electrospun Scaffolds, *Tissue Eng., Part A*, 2019, **25**(17), 1–16, DOI: 10.1089/ten.tea.2018.0306.

29 S. Adams, L. M. Wuescher, R. Worth and E. Yildirim-Ayan, Mechano-Immunomodulation: Mechanoresponsive Changes in Macrophage Activity and Polarization, *Ann. Biomed. Eng.*, 2019, DOI: 10.1007/s10439-019-02302-4.

30 J. Kluin, H. Talacua, A. I. P. M. Smits, *et al.*, In situ heart valve tissue engineering using a bioresorbable elastomeric implant – From material design to 12 months follow-up in sheep, *Biomaterials*, 2017, **125**, 101–117, DOI: 10.1016/j.biomaterials.2017.02.007.

31 G. C. Van Almen, H. Talacua, B. D. Ippel, *et al.*, Development of Non-Cell Adhesive Vascular Grafts Using Supramolecular Building Blocks, *Macromol. Biosci.*, 2016, **16**(3), 350–362, DOI: 10.1002/mabi.201500278.

32 D. E. P. Muylaert, G. C. van Almen, H. Talacua, *et al.*, Early *in situ* cellularization of a supramolecular vascular graft is modified by synthetic stromal cell-derived factor-1α derived peptides, *Biomaterials*, 2016, **76**, 187–195, DOI: 10.1016/j.biomaterials.2015.10.052.

33 L. A. Bockeria, O. Svanidze, A. Kim, *et al.*, Total cavopulmonary connection with a new bioabsorbable vascular graft: First clinical experience, *J. Thorac. Cardiovasc. Surg.*, 2017, **153**(6), 1542–1550, DOI: 10.1016/j.jtcvs.2016.11.071.

34 G. Bennink, S. Torii, M. Brugmans, *et al.*, A novel restorative pulmonary valved conduit in a chronic sheep model: Mid-term hemodynamic function and histologic assessment, *J. Thorac. Cardiovasc. Surg.*, 2018, **155**(6), 2591–2601, DOI: 10.1016/j.jtcvs.2017.12.046..

35 A. M. Schnell, S. P. Hoerstrup, G. Zund, *et al.*, Optimal cell source for cardiovascular tissue engineering: Venous vs. aortic human myofibroblasts, *Thorac. Cardiovasc. Surg.*, 2001, **49**(4), 221–225, DOI: 10.1055/s-2001-16113.

36 A. Mol, M. I. van Lieshout, C. G. Dam-de Veen, *et al.*, Fibrin as a cell carrier in cardiovascular tissue engineering applications, *Biomaterials*, 2005, **26**(16), 3113–3121, DOI: 10.1016/j.biomaterials.2004.08.007.

37 N. Grotenhuis, Y. Bayon, J. F. Lange, G. J. V. M. Van Osch and Y. M. Bastiaansen-Jenniskens, A culture model to analyze the acute biomaterial-dependent reaction of human primary macrophages, *Biochem. Biophys. Res. Commun.*, 2013, **433**(1), 115–120, DOI: 10.1016/j.bbrc.2013.02.054.

38 M. S. Shive, M. L. Salloum and J. M. Anderson, Shear stress-induced apoptosis of adherent neutrophils: a mechanism for persistence of cardiovascular device infections, *Proc. Natl. Acad. Sci. U. S. A.*, 2000, **97**, 6710–6715, DOI: 10.1073/pnas.110463197.

39 A. I. P. M. Smits, V. Ballotta, A. Driessen-Mol, C. V. C. Bouten and F. P. T. Baaijens, Shear flow affects selective monocyte recruitment into MCP-1-loaded scaffolds, *J. Cell. Mol. Med.*, 2014, **20**(10), 1–13, DOI: 10.1111/jcmm.12330.

40 F. Y. McWhorter, C. T. Davis and W. F. Liu, Physical and mechanical regulation of macrophage phenotype and function, *Cell. Mol. Life Sci.*, 2015, **72**(7), 1303–1316, DOI: 10.1007/s00018-014-1796-8.

41 M. R. Block, C. Badowski, A. Millon-Fremillon, *et al.*, Podosome-type adhesions and focal adhesions, so alike yet so different, *Eur. J. Cell Biol.*, 2008, **87**(8–9), 491–506, DOI: 10.1016/j.ejcb.2008.02.012.

42 S. J. Jenkins, D. Ruckerl, P. C. Cook, *et al.*, Local macrophage proliferation, rather than recruitment from the blood, is a signature of Th2 inflammation, *Science*, 2011, **332**(6035), 1284–1288, DOI: 10.1126/science.1204351.

43 A. Seneviratne, M. Hulsmans, P. Holvoet and C. Monaco, Biomechanical factors and macrophages in plaque stability, *Cardiovasc. Res.*, 2013, **99**(2), 284–293, DOI: 10.1093/cvr/cvt097.

44 A. N. Seneviratne, J. E. Cole, M. E. Goddard, *et al.*, Low shear stress induces M1 macrophage polarization in murine thin-cap atherosclerotic plaques, *J. Mol. Cell. Cardiol.*, 2015, **89**, 168–172, DOI: 10.1016/j.yjmcc.2015.10.034.

45 V. Ballotta, A. Driessen-Mol, C. V. C. Bouten and F. P. T. Baaijens, Strain-dependent modulation of macrophage polarization within scaffolds, *Biomaterials*, 2014, **35**(18), 4919–4928, DOI: 10.1016/j.biomaterials.2014.03.002.

46 W. Xuan, Q. Qu, B. Zheng, S. Xiong and G.-H. Fan, The chemotaxis of M1 and M2 macrophages is regulated by different chemokines, *J. Leukocyte Biol.*, 2015, **97**(1), 61–69, DOI: 10.1189/jlb.1A0314-170R.

47 S. A. Kellermann, S. Hudak, E. R. Oldham, Y. J. Liu and L. M. McEvoy, The CC Chemokine Receptor-7 Ligands 6Ckine and Macrophage Inflammatory Protein-3β Are Potent Chemoattractants for In Vitro- and In Vivo-Derived Dendritic Cells, *J. Immunol.*, 1999, **162**(7), 3859–3864.

48 J. C. Kling, M. Mack and H. Körner, The absence of CCR7 results in dysregulated monocyte migration and immunosuppression facilitating chronic cutaneous leishmaniasis, *PLoS One*, 2013, **8**(10), 1–16, DOI: 10.1371/journal.pone.0079098.

49 P. López-Cotarelo, C. Gómez-Moreira, O. Criado-García, L. Sánchez and J. L. Rodríguez-Fernández, Beyond Chemoattraction: Multifunctionality of Chemokine Receptors in Leukocytes, *Trends Immunol.*, 2017, **38**(12), 927–941, DOI: 10.1016/j.it.2017.08.004.

50 N. Sanchez-Sanchez, L. Riol-Blanco and J. L. Rodriguez-Fernandez, The Multiple Personalities of the Chemokine Receptor CCR7 in Dendritic Cells, *J. Immunol.*, 2006, **176**(9), 5153–5159, DOI: 10.4049/jimmunol.176.9.5153.

51 B. L. Eppert, G. T. Motz, B. W. Wortham, J. L. Flury and M. T. Borchers, CCR7 deficiency leads to leukocyte activation and increased clearance in response to pulmonary Pseudomonas aeruginosa infection, *Infect. Immun.*, 2010, **78**(5), 2099–2107, DOI: 10.1128/IAI.00962-09.

52 L. Buscemi, D. Ramonet, F. Klingberg, *et al.*, The single-molecule mechanics of the latent TGF-β1 complex, *Curr. Biol.*, 2011, **21**(24), 2046–2054, DOI: 10.1016/j.cub.2011.11.037.

53 N. R. Patel, M. Bole, C. Chen, *et al.*, Cell Elasticity Determines Macrophage Function, *PLoS One*, 2012, **7**(9), 1–10, DOI: 10.1371/journal.pone.0041024.

54 R. S. Labow, D. Sa, L. A. Matheson, D. L. M. Dinnes and J. P. Santerre, The human macrophage response during differentiation and biodegradation on polycarbonate-based polyurethanes: Dependence on hard segment chemistry, *Biomaterials*, 2005, **26**(35), 7357–7366, DOI: 10.1016/j.biomaterials.2005.05.048.

55 T. B. Wissing, V. Bonito, E. E. van Haaften, *et al.*, Macrophage-driven biomaterial degradation depends on scaffold microarchitecture, *Front. Bioeng. Biotechnol.*, 2019, **7**(April), 1–20, DOI: 10.3389/fbioe.2019.00087.

56 J. M. Anderson and A. K. McNally, Biocompatibility of implants: Lymphocyte/macrophage interactions, *Semin. Immunopathol.*, 2011, **33**(3), 221–233, DOI: 10.1007/s00281-011-0244-1.

57 D. M. Mosser and J. P. Edwards, Exploring the full spectrum of macrophage polarization, *Nat. Rev. Immunol.*, 2009, **8**(12), 958–969, DOI: 10.1038/nri2448.Exploring.

58 F. Ramirez and L. Y. Sakai, Biogenesis and function of fibrillin assemblies, *Cell Tissue Res.*, 2010, **339**(1), 71–82, DOI: 10.1007/s00441-009-0822-x.

59 P. Y. Lee, Y. C. Liu, M. X. Wang and J. J. Hu, Fibroblast-seeded collagen gels in response to dynamic equibiaxial mechanical stimuli: A biomechanical study, *J. Biomech.*, 2018, **78**(sep), 134–142, DOI: 10.1016/j.jbiomech.2018.07.030.

60 K. S. Park, E. G. Lee and Y. Son, Uniaxial cyclic strain stimulates cell proliferation and secretion of interleukin-6 and vascular endothelial growth factor of human dermal fibroblasts seeded on chitosan scaffolds, *J. Biomed. Mater. Res., Part A*, 2014, **102**(7), 2268–2276, DOI: 10.1002/jbm.a.34881.

61 A. Mol, C. V. C. Bouten, G. Zünd, *et al.*, The relevance of large strains in functional tissue engineering of heart valves, *Thorac. Cardiovasc. Surg.*, 2003, **51**(2), 78–83, DOI: 10.1055/s-2003-38993.

62 M. Stekelenburg, M. C. M. Rutten, L. H. E. H. Snoeckx and F. P. T. Baaijens, Dynamic Straining Combined with Fibrin Gel Cell Seeding Improves Strength of Tissue-Engineered Small-Diameter Vascular Grafts, *Tissue Eng., Part A*, 2009, **15**(5), 1081–1089, DOI: 10.1089/ten.tea.2008.0183.

63 Z. D. Shi, G. Abraham and J. M. Tarbell, Shear Stress Modulation of Smooth Muscle Cell Marker Genes in 2-D and 3-D Depends on Mechanotransduction by Heparan Sulfate Proteoglycans and ERK1/2, *PLoS One*, 2010, **5**(8), 1–9, DOI: 10.1371/journal.pone.0012196.

64 A. Schildberger, E. Rossmanith, T. Eichhorn, K. Strassl and V. Weber, Monocytes, peripheral blood mononuclear cells, and THP-1 cells exhibit different cytokine expression pat-

 

terns following stimulation with lipopolysaccharide, *Mediators Inflammation*, 2013, **2013**, 697972, DOI: 10.1155/2013/697972.

65 R. S. Labow, Y. Tang, C. B. McCloskey and J. P. Santerre, The effect of oxidation on the enzyme-catalyzed hydrolytic biodegradation of poly(urethane)s, *J. Biomater. Sci., Polym. Ed.*, 2002, **13**(6), 651–665, DOI: 10.1163/156856202320269148.

66 J. E. McBane, J. P. Santerre and R. S. Labow, Role of protein kinase C in the monocyte-derived macrophage-mediated biodegradation of polycarbonate-based polyurethanes, *J. Biomed. Mater. Res., Part A*, 2005, **74**(1), 1–11, DOI: 10.1002/jbm.a.30311.

67 R. S. Labow, E. Meek and J. P. Santerre, Model systems to assess the destructive potential of human neutrophils and monocyte-derived macrophages during the acute and chronic phases of inflammation, *J. Biomed. Mater. Res.*, 2001, **54**(2), 189–197, DOI: 10.1002/1097-4636(200102)54:2<189::AID-JBM5>3.0.CO;2-8.